Modeling of Particle Evolution in Aerosol Reactors with Coflowing Gaseous Reactants

Andreas Bensberg, Paul Roth, Reinhard Brink, and Helmut Lange
Institut für Verbrennung und Gasdynamik, Universität Duisburg, 47048 Duisburg, Germany

A simple model is presented for simultaneous nucleation and coagulation in combination with convective and diffusive particle transport in gas-phase aerosol reactors over the entire particle-size spectrum. This model is applied to a spatially inhomogeneous aerosol reactor. The flow and reaction characteristics correspond to a confined coflow diffusion flame of $SiCl_4$ and NH_3 in a wall-heated flow. The reactor geometry and the initial and boundary conditions suggest the application of the boundary layer approximations. The reaction process is described by the flame-sheet model. The particle-size spectrum is approximated by a unimodal lognormal function. The characteristics of the SiN_4 aerosol (concentration, polydispersity, and average particle size) calculated at every point in the reactor vary significantly in space. At the position of the reaction zone in the outlet cross section, for example, the average particle radius is small ($r_g \approx 1$ nm) and the standard deviation is large ($\sigma > 2$). At other radial positions the particles are much larger ($r_g \approx 15$ nm) and the size distribution is almost self-preserving ($\sigma \approx 1.36$).

Introduction

Aerosol reactors are used for production of nanosize particles such as carbon blacks, pigments, optical fibers, and advanced ceramics (see Ulrich, 1971; Chung and Katz, 1985; Pratsinis and Mastrangelo, 1989; Kim, 1997; Xing et al., 1996). In industrial applications they are often produced by gas-phase chemical reaction in the way that precursors are issued in two separated concentric gas flows. The structure of the flow and reaction processes resemble a laminar coflow diffusion flame in axisymmetric geometries; see Figure 1. These reactors are notoriously nonuniform aerosol generation systems. The result is a complex interplay of chemical reaction, nucleation, coagulation, and convective and diffusive transport. For optimal design and operation of these reactors a mathematical reactor model is needed, which, on the one hand, is sufficiently detailed to capture the complexity of the inner processes, while, on the other hand, the model has to be simple enough to be feasible for numerical evaluation. To fulfill the requirements several assumptions are made. The length L_R of the reactor is usually much larger than its radius r_R, that is, $L_R \gg r_R$, and the reaction zone extends over a large part of the reactor length. This suggests the application of the boundary-layer approximations. Since flow and reaction characteristics resemble a laminar coflow diffusion flame, the chemical reaction is usually fast compared to species diffusion. Additionally, kinetic data are not suffi-

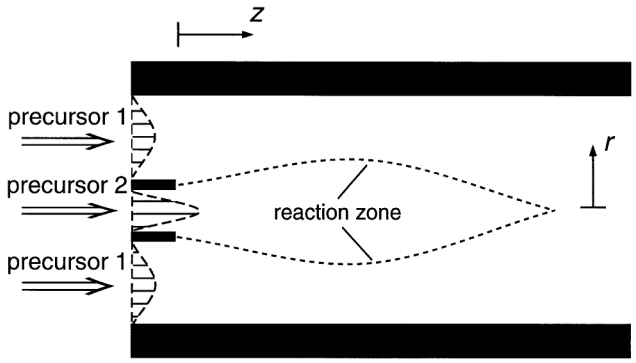

Figure 1. Reactor model.

Correspondence concerning this article should be addressed to P. Roth.
Present address of H. Lange: Bayer AG, AI-ASG/R82, 47812 Krefeld, Germany.

ciently available to describe the chemical reaction in detail. This leads to the application of the flame-sheet model, which corresponds to the assumption of an infinitely fast chemical reaction. Furthermore, the supersaturation of the condensable species is sufficiently high such that the particle growth occurs via diffusion-limited aggregation (DLA) with single molecules acting as primary particles (Ulrich, 1971, 1984). In this case, the nucleation rate equals the gas-phase reaction rate. The particles further grow only by Brownian coagulation. The shape of the resulting aerosol-size distribution is approximated by a unimodal lognormal function. This type of treatment was successfully applied to particle coagulation problems for the free molecule regime (Lee et al., 1984) and for the continuum plus near continuum regime (Whitby et al., 1991; Lee et al., 1997).

In the present work the momentum method is applied to the formation of Si_3N_4 particles in a wall-heated tube reactor and extended to spatially inhomogeneous processes including particle diffusion. The three moments of the size distribution have to be calculated and the three parameters can be determined uniquely. Balance equations for these moments can be derived from the particle dynamic equation (Friedlander, 1977). Experiments on Si_3N_4 synthesis in furnaces and laser reactors are known (Prochazka and Greskovich, 1978; Janiga et al., 1991; Kizaki et al., 1985; Kruis et al., 1998; Danforth, 1992), but the reaction conditions are quite different from the present ones.

Theory

Particle-dynamic equation

The particle-size distribution $N(r_p)$ is assumed to be continuous such that $N(r_p)dr_p$ is the number density of particles with radii between r_p and $r_p + dr_p$. Neglecting external and electrical force fields the particle-dynamic equation (PDE) describing the spatial and temporal evolution of $N(r_p)$ can be written as (Friedlander, 1977)

$$\frac{\partial N}{\partial t} + \nabla\cdot(\boldsymbol{v}_{p,r}N) = \frac{J}{m_{p0}}\delta(r_p - r_{p0}) + \frac{1}{2}\int_{\bar{r}_p=0}^{r_p}\beta\left[\bar{r}_p,\left(r_p^3-\bar{r}_p^3\right)^{1/3}\right]N(\bar{r}_p)\,N\left[\left(r_p^3-\bar{r}_p^3\right)^{1/3}\right]d\bar{r}_p - N(r_p)\int_{\bar{r}_p=0}^{\infty}\beta(\bar{r}_p,r_p)\,N(\bar{r}_p)\,d\bar{r}_p, \quad (1)$$

where $\boldsymbol{v}_{p,r}$ is the velocity of particles with radii between r_p and $r_p + dr_p$; J is the specific mass production of critical clusters; m_{p0} is the mass of critical clusters, that is, particles of the critical radius r_{p0}; and β is the collision frequency function. Quantities such as $\boldsymbol{v}_{p,r}$, J, and β also depend on space and time. For convenience this is not stated explicitly in the list of variables. The terms on the lefthand side represent the local temporal rate of change in N and the change due to convective particle transport. The first term on the righthand side represents the production of critical clusters per unit time. The second and third terms account for the gain and loss of particles within a size interval due to coagulation (Friedlander, 1977). Since the particles are primarily transported with the mean aerosol flow, the particle movement relative to the mean velocity of the aerosol is described by a diffusion approach. Such an approach describes the relative motion between particles and gas. Hence, a diffusion law of the Fickian type reads

$$N(\boldsymbol{v}_{p,r} - \boldsymbol{v}_G) = -D_r\nabla N, \quad (2)$$

where $\boldsymbol{v}_G$ is the gas velocity and D_r the diffusion coefficient for particles with radius r_p. Based on the Stokes–Einstein expression for the continuum regime and extended to the free molecular regime by a correction due to Cunningham, D_r is given by

$$D_r = \frac{k_B T}{6\pi\mu_G r_p}(1 + AKn), \quad (3)$$

where k_B is the Boltzmann constant; T the Kelvin temperature; μ_G the viscosity of the gas phase; $A = 1.657$ a constant; and Kn the Knudsen number of the particles, which is defined as $Kn = l_G/r_p$, where l_G is the mean free path of the gas molecules. The term $\boldsymbol{v}_{p,r}N$ in the PDE can be written as

$$\boldsymbol{v}_{p,r}N = \boldsymbol{v}N - D_r\nabla N + \boldsymbol{u}_G N, \quad (4)$$

where $\boldsymbol{v}$ is the aerosol velocity and $\boldsymbol{u}_G$ the velocity of the gas phase relative to the aerosol. The PDE can then be rewritten as

$$\frac{\partial N}{\partial t} + \nabla\cdot(\boldsymbol{v}N) - \nabla\cdot(D_r\nabla N - \boldsymbol{u}_G N) = \frac{J}{m_{p0}}\delta(r_p - r_{p0}) + \frac{1}{2}\int_{\bar{r}_p=0}^{r_p}\beta\left[\bar{r}_p,\left(r_p^3-\bar{r}_p^3\right)^{1/3}\right]N(\bar{r}_p)\,N\left[\left(r_p^3-\bar{r}_p^3\right)^{1/3}\right]d\bar{r}_p - N(r_p)\int_{\bar{r}_p=0}^{\infty}\beta(\bar{r}_p,r_p)\,N(\bar{r}_p)\,d\bar{r}_p. \quad (5)$$

The size distribution of the particles is approximated by a lognormal function of the form (Friedlander, 1977):

$$N(r_p) = \frac{N_p}{\sqrt{2\pi}\ln\sigma}\exp\left\{-\frac{1}{2}\left[\frac{\ln(r_p/r_g)}{\ln\sigma}\right]^2\right\}\frac{1}{r_p}, \quad (6)$$

where N_p is the total number density of particles, r_g the geometric particle radius, and σ the standard deviation. It should be noted that, although the assumption just employed restricts the solution to the form of a lognormal function, the three size parameters of the distribution N_p, r_g, and σ are allowed to vary in space and time. Many experimental results and numerical calculations indicate that particle-size distributions during coagulation indeed fit a lognormal function. Even if a distribution is found not to be truly lognormal, it is customary to represent calculated or measured size distributions with equivalent geometric-size parameters such as N_p,

r_g, and σ that are computed from the discrete-size spectrum. The spatial and temporal evolution of these three parameters is determined by calculating three moments of the size distribution.

The kth moment of a size distribution $N(r_p)$ is defined by

$$M_k = \int_0^\infty r_p^k N(r_p)\, dr_p, \tag{7}$$

where k is a real number. In the case of a lognormal size distribution function the integral can be evaluated to be

$$M_k = N_p r_g^k \exp\left(\frac{1}{2}k^2 \ln^2 \sigma\right). \tag{8}$$

Balance equations for the moments can be derived from the PDE to give

$$\frac{\partial M_k}{\partial t} + \nabla\cdot(\boldsymbol{v}M_k) + \nabla\cdot\left(\boldsymbol{j}_{M_k} + \boldsymbol{u}_G M_k\right) = \frac{r_{p0}^k J}{m_{p0}} + P_k, \tag{9}$$

$$P_k = \frac{1}{2}\int_0^\infty\int_0^\infty \left[\left(r_{p1}^3 + r_{p2}^3\right)^{k/3} - r_{p1}^k - r_{p2}^k\right] \times \beta(r_{p1}, r_{p2}) N(r_{p1}) N(r_{p2}) dr_{p1}\, dr_{p2}, \tag{10}$$

where $\boldsymbol{j}_{M_k}$ is the diffusion flux of the kth moment. In the case of a lognormal size distribution function, $\boldsymbol{j}_{M_k}$ can be calculated to be

$$\boldsymbol{j}_{M_k} = -D_{M_k}\nabla M_k - M_k D_C \left\{\nabla\left[\frac{\exp\left[\frac{1}{2}(1-2k)\ln^2\sigma\right]}{r_g}\right] + Al_G\nabla\left[\frac{\exp\left[2(1-k)\ln^2\sigma\right]}{r_g^2}\right]\right\}, \tag{11}$$

where

$$D_{M_k} = \frac{kT}{6\pi\mu_G r_g}\left\{\exp\left[\frac{1}{2}(1-2k)\ln^2\sigma\right] + AKn_g \exp\left[2(1-k)\ln^2\sigma\right]\right\} \tag{12}$$

$$D_C = \frac{kT}{6\pi\mu_G}, \qquad Kn_g = \frac{l_G}{r_g}. \tag{13}$$

Particularly in the case of the flame-sheet model, the parameter N_p has steep gradients near the flame-sheet, while the gradients of the other two parameters r_g and σ are comparatively smooth. Since M_k is proportional to N_p the moments have steep gradients near this point, too. This motivates the approximation only to consider the first term on the righthand side of Eq. 11. The diffusion law then reduces to a Fickian-type diffusion flux for the kth moment of the form

$$\boldsymbol{j}_{M_k} \cong -D_{M_k}\nabla M_k. \tag{14}$$

The relative velocity of the gas phase can be calculated as

$$u_G = \frac{4\pi}{3}\frac{\rho_p^o}{\rho} D_C \left\{\nabla\left[r_g^2 \exp\left(2\ln^2\sigma\right)\right] + Al_G\nabla\left[r_g \exp\left(\frac{1}{2}\ln^2\sigma\right)\right]\right\}, \tag{15}$$

where ρ_p^o is the density of the particle material and ρ the averaged aerosol density.

To obtain a closed set of balance equations for the moments, the last term in Eq. 9, the collision integral, has to be evaluated. This can be best performed if k is a multiple of three. In particular for $k = 3$ the integrand vanishes. So, coagulation has no impact on the third moment. This is not surprising, because the third moment represents the mass density of the particle phase and this quantity is not changed by coagulation. Since three moments have to be calculated in order to determine the evolution of three parameters N_p, r_g, and σ, the moments M_0, M_3, and M_6 are chosen. The collision integral P_k in Eq. 10 has to be evaluated for $k = 0, 3, 6$. The gas–particle interaction is completely different for the free molecular size regime and for the continuum regime, and so are the collision frequency functions. For the free molecular regime (FM) the collision frequency function is

$$\beta_{FM}(r_{p1}, r_{p2}) = \left(\frac{6kT}{\rho_p^o}\right)^{1/2}(r_{p1} + r_{p2})^2\left(\frac{1}{r_{p1}^3} + \frac{1}{r_{p2}^3}\right)^{1/2}. \tag{16}$$

For $k = 0$ and the lognormal distribution given in Eq. 6 the integral can be evaluated partially up to the expression:

$$P_0^{FM} = -N_p^2\left(\frac{6r_g kT}{\pi\rho_p^o}\right)^{1/2}\exp\left(\frac{Z}{16}\right) \times \int_{-\infty}^{\infty}\left[1 + \exp\left(2\sqrt{Z}\,y\right)\right] \times \left[\exp\left(3\sqrt{Z}\,y\right) + \exp\left(-3\sqrt{Z}\,y\right)\right]^{1/2}\exp\left(-y^2\right)dy, \tag{17}$$

where T, N_p, r_g, and $Z = \ln^2\sigma$ are functions of $\boldsymbol{x}$ and t. The remaining integral cannot be solved exactly, but some attempts exist to calculate it approximately (Pratsinis, 1988; Otto et al., 1997). The authors found a more precise approximation, as is shown in the Appendix. The collision integral is

then calculated to be

$$P_0^{FM} = -\xi_{FM} M_0^2, \tag{18}$$

where

$$\xi_{FM} = \left(\frac{6 r_g kT}{\rho_p^o}\right)^{1/2} \exp\left(\frac{Z}{8}\right)\left\{\exp(3Z) + 2\exp\left(\frac{Z}{2}\right) + 1 - \frac{1-\sqrt{2}/2}{\sqrt{W}} \exp\left(-\frac{W-1}{W}\frac{Z}{16}\right) \times \left[\exp\left(3\frac{Z}{W}\right) + 2\exp\left(\frac{Z}{2W}\right) + 1\right]\right\} \tag{19}$$

$$W = 1 + \frac{9}{4}\ln^2 \sigma.$$

Using the same approximation, the collision integral for $k = 6$ becomes

$$P_6^{FM} = \eta_{FM} M_3^2, \tag{20}$$

where

$$\eta_{FM} = 2\left(\frac{6 r_g kT}{\rho_p^o}\right)^{1/2} \exp\left(\frac{13}{8}Z\right)\left\{\exp(3Z) + 2\exp\left(\frac{Z}{2}\right) + 1 - \frac{1-\sqrt{2}/2}{\sqrt{W}} \exp\left(-\frac{W-1}{W}\frac{Z}{16}\right) \times \left[\exp\left(3\frac{Z}{W}\right) + 2\exp\left(\frac{Z}{2W}\right) + 1\right]\right\}. \tag{21}$$

If the particles are assumed to be spherical, the collision frequency function for the continuum regime (C) reads

$$\beta_C(r_{p1}, r_{p2}) = \frac{2kT}{3\mu_G}(r_{p1} + r_{p2})\left(\frac{C(r_{p1})}{r_{p1}} + \frac{C(r_{p2})}{r_{p2}}\right), \tag{22}$$

$$C(r_p) = 1 + BKn, \qquad B = 1.56.$$

For this regime the integral in Eq. 10 can exactly be calculated as

$$P_0^C = -\xi_C M_0^2, \qquad P_6^C = -\eta_C M_3^2, \tag{23}$$

where

$$\xi_C = \frac{2kT}{3\mu_G}\left\{1 + \exp(Z) + BKn_g \exp\left(\frac{Z}{2}\right)[1 + \exp(2Z)]\right\} \tag{24}$$

$$\eta_C = \frac{4kT}{3\mu_G}\left\{1 + \exp(Z) + BKn_g \exp\left(-\frac{Z}{2}\right)[1 + \exp(-2Z)]\right\}. \tag{25}$$

To also cover the transition regime between free molecular and continuum conditions, the harmonic mean approximation is used. This approach was taken previously by Pratsinis (Pratsinis, 1988). The collision integral is then calculated by just one expression for each moment. For the zeroth moment this is

$$P_0 = -\xi N_p^2, \tag{26}$$

where

$$\frac{1}{\xi} = \frac{1}{\xi_{FM}} + \frac{1}{\xi_C}, \tag{27}$$

and for the 6th moment

$$P_6 = -\eta \rho_p^2, \tag{28}$$

where

$$\frac{1}{\eta} = \frac{1}{\eta_{FM}} + \frac{1}{\eta_C}. \tag{29}$$

Balance equations

The aerosol is treated as an ideal suspension of gas and particles for which the continuum equations are to be valid. Neglecting external and electrical force fields as well as radiative heat transfer, the balance equations for mass, momentum, and energy of the aerosol, and for the gas species read:

$$\frac{\partial \rho}{\partial t} + \nabla\cdot(\rho \boldsymbol{v}) = 0 \tag{30}$$

$$\frac{\partial \rho \boldsymbol{v}}{\partial t} + \nabla\cdot(\rho \boldsymbol{v}\boldsymbol{v} - \boldsymbol{t}) = 0 \tag{31}$$

$$\frac{\partial \rho h}{\partial t} - \frac{\partial p}{\partial t} + \nabla\cdot(\rho \boldsymbol{v} h + \boldsymbol{q}) - \boldsymbol{v}\cdot\nabla p - \boldsymbol{\sigma}:\nabla \boldsymbol{v} = 0 \tag{32}$$

$$\frac{\partial \rho Y_{G_\alpha}}{\partial t} + \nabla\cdot(\rho \boldsymbol{v} Y_{G_\alpha} + \boldsymbol{j}_{G_\alpha}) = 0, \tag{33}$$

where $\boldsymbol{t}$ and σ are the stress tensor and its contribution due to friction; h, p and $\boldsymbol{q}$ are the specific enthalpy, the pressure, and the heat flux, respectively. Y_{G_α} and j_{G_α} are the mass fraction of the gas species α and its diffusion flux. The gas phase is considered as a mixture of ideal gases. The particles are assumed to be incompressible and to have a constant heat capacity. For the stress and the heat flux of the gas phase, the material laws of Newton and Fourier are applied. The particle phase is assumed not to contribute to the stress and the heat flux of the aerosol. Then the material laws for the stress and the heat flux of the aerosol read:

$$\boldsymbol{t} = -p\boldsymbol{I} + (1 - \epsilon_p)\mu_G\left(\nabla \boldsymbol{v} + \nabla^T \boldsymbol{v} - \frac{2}{3}\nabla\cdot \boldsymbol{v}\boldsymbol{I}\right) \tag{34}$$

$$\boldsymbol{q} = -(1 - \epsilon_p)\lambda_G \nabla T + \sum_\alpha (j_{G_\alpha} + \rho \boldsymbol{u}_G) h_{G_\alpha} - \rho(1 - Y_p)\boldsymbol{u}_G h_p, \tag{35}$$

where ϵ_p is the volume fraction of the particle phase, Y_p the mass fraction of the particle phase, and h_{G_α} and h_p are the specific enthalpies of the gas species α and of the particle phase, respectively. The gas species participating in chemical reaction are assumed to be highly diluted by a chemically inert gas. Then the diffusion flux j_{G_α} of the reacting gas species can be described by Fick's law:

$$j_{G_\alpha} = -\left(1 - Y_p\right)\rho\left(D_{G_\alpha}\nabla Y_{G_\alpha} - \boldsymbol{u}_G\right), \tag{36}$$

where D_{G_α} is the coefficient of diffusion of the species α into the gas mixture.

The transport coefficients μ_G, λ_G, and D_{G_α} in the preceding equations are calculated on the basis of the kinetic theory of gases for the interaction potential of hard sphere molecules. A useful empirical formula for μ_G with some theoretical justification (Hirschfelder et al., 1954) is

$$\mu_G = \sum_\alpha \frac{X_\alpha}{X_\alpha/\mu_{G_\alpha} + 1.385\sum\limits_{\beta\neq\alpha}\left(X_\beta k_B T\right)/\left(pm_o M_\alpha D_{\alpha\beta}\right)}, \tag{37}$$

where X_α and M_α are the mole fraction and the molar weight of species α, and m_o is the mass of a hydrogen atom. The formulas for the viscosity μ_{G_α} of the pure species and for the binary diffusion coefficient $D_{\alpha\beta}$ are

$$\mu_{G_\alpha} = \frac{5}{32}\sqrt{\frac{m_o M_\alpha k_B T}{2\pi}}\,\frac{1}{r_\alpha^2} \tag{38}$$

$$D_{\alpha\beta} = \frac{kT}{p}\sqrt{\frac{k_B T}{8\pi m_o M_{\alpha\beta}}}\,\frac{1}{\left(r_\alpha^2 + r_\beta^2\right)^2}, \tag{39}$$

where r_α is the radius of the hard spheres and $M_{\alpha\beta}$ is defined by

$$M_{\alpha\beta} = \frac{M_\alpha M_\beta}{M_\alpha + M_\beta}. \tag{40}$$

The thermal conductivity λ is calculated by the combination averaging formula of the pure species conductivities λ_α (Mathur et al., 1967):

$$\lambda = \frac{1}{2}\left(\sum_\alpha X_\alpha\lambda_\alpha + \frac{1}{\sum\limits_\alpha \frac{X_\alpha}{\lambda_\alpha}}\right),$$

$$\lambda_\alpha = \left(c_p^\alpha + \frac{9}{4}\frac{R}{M_\alpha}\right)\mu_{G_\alpha}, \tag{41}$$

where R is the universal gas constant. Finally, the diffusion coefficient is calculated by

$$D_\alpha = \frac{1 - X_\alpha}{\sum\limits_{\beta\neq\alpha} X_\beta/D_{\alpha\beta}}. \tag{42}$$

To achieve good agreement with experimental results, the hard sphere radii are calculated on the basis of Eq. 38, where experimentally determined values for μ_{G_α} at an estimated mean temperature of the aerosol reactor are taken. Although the interaction potential for hard-sphere molecules is quite simple, the preceding formulas for the transport coefficients of the gas phase are well suited to describe the dependence of these coefficients on temperature and composition of the gas mixture.

In the material laws, Eqs. 37 to 39, the mass fraction Y_p and the volume fraction ϵ_p of the particle phase appear. These also depend on space and time. However, if the third moment and the aerosol density are known, they can be calculated by

$$Y_p = \frac{4\pi}{3}\frac{\rho_p^0}{\rho}M_3, \qquad \epsilon_p = \frac{4\pi}{3}M_3. \tag{43}$$

As stated earlier, the balance equations are valid for regular points in the flow field. The flame-sheet model produces an internal boundary where the balance equations for singular points have to be applied. In the case of a stationary boundary they read:

$$[\,\rho\boldsymbol{v}]\cdot\boldsymbol{n}_F = 0 \tag{44}$$

$$[\,\rho\boldsymbol{v}\boldsymbol{v} - \boldsymbol{t}]\cdot\boldsymbol{n}_F = 0 \tag{45}$$

$$\left[\,\rho\left(h + \frac{1}{2}v^2\right)\boldsymbol{v} + \boldsymbol{q} - \boldsymbol{v}\cdot\boldsymbol{\sigma}\right]\cdot\boldsymbol{n}_F = 0 \tag{46}$$

$$[\,\rho\boldsymbol{v}Y_{G_\alpha} - \boldsymbol{j}_{G_\alpha}]\cdot\boldsymbol{n}_F = \omega_\alpha \tag{47}$$

$$[\boldsymbol{v}M_k + \boldsymbol{j}_{M_k} + \boldsymbol{u}_G M_k]\cdot\boldsymbol{n}_F = \frac{r_{p0}^k J}{m_{p0}}. \tag{48}$$

where $\boldsymbol{n}_F$ is the unit normal vector on the flame sheet; ω_α is the mass production of the gas species α in the flame sheet; and J is the mass production of the particle phase in the flame sheet. The brackets $[f]$ represent the difference between the lefthand side limit and the righthand side limit of the argument f at the flame-sheet position. This difference is either zero, if the argument function is continuous, or equal to the righthand side source terms.

In the present case, we consider only the stationary operation of a rotationally symmetric reactor. Applying boundary-layer approximations the system of balance equations reads in cylindrical coordinates for regular points:

$$\frac{\partial r\rho v_r}{\partial r} + \frac{\partial r\rho v_z}{\partial z} = 0 \tag{49}$$

$$\frac{\partial p}{\partial r} = 0 \tag{50}$$

$$\rho v_r \frac{\partial v_z}{\partial r} + \rho v_z \frac{\partial v_z}{\partial z} + \frac{\partial p}{\partial z} - \frac{1}{r}\frac{\partial}{\partial r}\left[r(1-\epsilon_p)\mu_G \frac{\partial v_z}{\partial r}\right] = 0 \qquad (51)$$

$$\rho v_r c_p \frac{\partial T}{\partial r} + \rho v_z c_p \frac{\partial T}{\partial z} - \frac{1}{r}\frac{\partial}{\partial r}\left[r(1-\epsilon_p)\lambda_G \frac{\partial T}{\partial r}\right] + (1-Y_p)\rho\left\{ \left[c_p - (1+Y_p)c_p^p \right] u_r^G - \sum_\alpha c_p^{G_\alpha} D_\alpha \frac{\partial Y_\alpha}{\partial r}\right\}\frac{\partial T}{\partial r} - v_z \frac{\partial p}{\partial z} - (1-\epsilon_p)\mu_G\left(\frac{\partial v_z}{\partial r}\right)^2 = 0 \qquad (52)$$

$$\rho\left(v_r + u_r^G\right)\frac{\partial Y_\alpha}{\partial r} + \rho v_z \frac{\partial Y_\alpha}{\partial z} - \frac{1}{r(1-Y_p)}\frac{\partial}{\partial r}\left[r(1-Y_p)\rho D_\alpha \frac{\partial Y_\alpha}{\partial r}\right] = 0 \qquad (53)$$

$$\frac{\partial v_r M_0}{\partial r} + \frac{\partial v_z M_0}{\partial z} - \frac{1}{r}\frac{\partial}{\partial r}\left(r D_{M_0}\frac{\partial M_0}{\partial r} - r u_r^G M_0\right) = -\xi M_0^2 \qquad (54)$$

$$\frac{\partial v_r M_3}{\partial r} + \frac{\partial v_z M_3}{\partial z} - \frac{1}{r}\frac{\partial}{\partial r}\left(r D_{M_3}\frac{\partial M_3}{\partial r} - r u_r^G M_3\right) = 0 \qquad (55)$$

$$\frac{\partial v_r M_6}{\partial r} + \frac{\partial v_z M_6}{\partial z} - \frac{1}{r}\frac{\partial}{\partial r}\left(r D_{M_6}\frac{\partial M_6}{\partial r} - r u_r^G M_6\right) = \eta M_3^2, \qquad (56)$$

where $c_p^{G_\alpha}$ and c_p^p are the specific heat capacities of the gas species α and of the particle phase, respectively. The specific heat capacity c_p of the aerosol is calculated by

$$c_p = (1-Y_p)\sum_\alpha Y_{G_\alpha} c_p^{G_\alpha} + Y_p c_p^p. \qquad (57)$$

The flame-sheet model implies the assumption that all quantities are continuous at the flame sheet. This does generally not hold for their gradients. To fix ideas we consider a one-step irreversible chemical reaction of the type:

$$\nu_1 G_1 + \nu_2 G_2 \rightarrow |\nu_3| G_3 + |\nu_P| P, \qquad (58)$$

where G_1, G_2 represent the precursors; G_3 a gaseous reaction product; and P the condensable molecular species. The two precursors diffuse from different sides toward the flame sheet. At this point they react completely so that their mass fractions are zero there. They do not penetrate the flame sheet and beyond the flame sheet their mass fractions are zero. Principally, one or more precursors can be added if their diffusion coefficients are significantly larger than those of the other two precursors. One example of such an additional third precursor could be hydrogen (H_2).

The preceding assumptions and the thereby simplified singular balance equations (Eqs. 44–48) then read

$$[\rho] = [v_r] = [v_z] = [T] = [p] = [Y_\alpha] = [M_k] = 0 \qquad (59)$$

$$\left[\frac{\partial v_z}{\partial r}\right] = 0 \qquad (60)$$

$$\lambda_G\left[\frac{\partial T}{\partial r}\right] = \Delta_R H \Lambda \qquad (61)$$

$$-(1-Y_p)\rho D_\alpha\left[\frac{\partial Y_\alpha}{\partial r}\right] = \omega_\alpha + Y_\alpha J \qquad (62)$$

$$-D_{M_k}\left[\frac{\partial M_k}{\partial r}\right] - \frac{J}{(1-Y_p)\rho}M_k = \frac{r_{p0}^k J}{m_{p0}}, \qquad (63)$$

where $\Delta_R H$ is the molar heat of reaction; Λ is the reaction rate in moles per second; and ω_α is the mass production rate of species α, which can be expressed by the reaction rate as

$$\omega_\alpha = -\nu_\alpha M_\alpha \Lambda, \qquad \alpha = 1,2 \qquad (64)$$

$$\omega_3 = \nu_3 M_3 \Lambda, \qquad J = -\nu_p M_p \Lambda. \qquad (65)$$

The reaction rate is

$$\Lambda = \left| (1-Y_p)\frac{\rho D_1}{\nu_1 M_1}\left(\frac{\partial Y_1}{\partial r}\right)\right|_{r=r_F}\Bigg|, \qquad (66)$$

where r_F is the radial position of the flame sheet and $(\partial Y_1/\partial r)|_{r=r_F}$ denotes the derivative of Y_1 at the flame sheet.

Numerical Method

The preceding system of parabolic differential equations is stepwise integrated in the z-direction. The procedure begins at the inlet where initial conditions are stated. The discretization is performed by finite differences. Stability problems of the system of differential equations, which are mainly caused by the source terms due to coagulation in the balance equations of the zeroth and the 6th moment, require an implicit numerical scheme. For the derivatives with respect to the radius second-order difference approximations can be applied everywhere except at the flame sheet. In the flame sheet the derivatives of the moments are so steep that they must be approximated by difference formulas of first order. Derivatives with respect to z are also approximated by difference formulas of first order. The pressure gradient $\partial p/\partial z$ in the balance equations for momentum and energy is not eliminated by use of the ideal gas law but determined iteratively. The iteration method makes use of the conservation of the total mass flux in the z-direction.

Results and Discussion

Initial and boundary conditions

Initial conditions are prescribed at the inlet of the reactor. The two precursors are injected into the reactor separately in two concentric flows: an inner flow injected through a nozzle and an outer annulus flow. Each of them is diluted by an inert gas. The initial velocity profiles are given as solutions of

the incompressible Navier–Stokes equations, for example, Hagen–Poiseuille. The concentration is homogeneous in each flow, and temperature and pressure are also homogeneous and equal in the two flows. The radial velocity is set equal to zero.

The walls of the reactor are assumed to be adiabatic. There will be no mass flux into or out of the wall, and the no-slip condition is assumed. Hence, the gradients of the temperature, of the species mass fractions, and of the moments as well as both components of the velocity themselves are zero at the wall. For reasons of symmetry the gradients of temperature, species mass fractions, moments, and velocity in the z-direction as well as the velocity in the r-direction itself are zero at the symmetry axis ($r = 0$), too. Thus, the boundary conditions are

$$\left.\frac{\partial T}{\partial r}\right|_{r=0} = 0 \qquad \left.\frac{\partial T}{\partial r}\right|_{r=r_R} = 0 \tag{67}$$

$$\left.\frac{\partial Y_\alpha}{\partial r}\right|_{r=0} = 0 \qquad \left.\frac{\partial Y_\alpha}{\partial r}\right|_{r=r_R} = 0 \tag{68}$$

$$\left.\frac{\partial M_k}{\partial r}\right|_{r=0} = 0 \qquad \left.\frac{\partial M_k}{\partial r}\right|_{r=r_R} = 0, \quad k = 0,3,6 \tag{69}$$

$$v_z|_{r=0} = 0 \qquad \left.\frac{\partial v_z}{\partial r}\right|_{r=r_R} = 0 \tag{70}$$

$$v_r|_{r=0} = 0 \qquad v_r|_{r=r_R} = 0. \tag{71}$$

Examples

The formation of silicon nitride (Si_3N_4) in a typical laboratory reactor is considered. The gas-phase precursors used are silicon tetrachloride ($SiCl_4$) and ammonium (NH_3), which both are diluted by the inert gas nitrogen (N_2). A one-step reaction is assumed:

$$4\,NH_3 + 3\,SiCl_4 \rightarrow 12\,HCl + Si_3N_4, \tag{72}$$

where Si_3N_4 is considered as a hypothetical molecular particle. In the following, the indices 1 to 4 refer to NH_3, $SiCl_4$, HCl, N_2, respectively. The molar heat of reaction is assumed to be

$$\Delta_R H \approx -257 \text{ kJ/mol}. \tag{73}$$

The density of the amorphous particle material is estimated to be $\rho_p^o = 2600$ kg/m^3. The specific heat capacities used are taken from the JANAF thermochemical tables (Chase et al., 1985):

$$c_p^{G_1} = 3{,}301.65 \text{ J/kg·K}, \quad c_p^{G_2} = 755.1 \text{ J/kg·K},$$
$$c_p^{G_3} = 857.81 \text{ J/kg·K}, \quad c_p^{G_4} = 1{,}169.5 \text{ J/kg·K},$$
$$c_p^p = 2{,}305.4 \text{ J/kg·K}. \tag{74}$$

The radius of the reactor r_R and the inner and outer radii r_{I1} and r_{I2} of the nozzle through which the inner flow is injected are

$$r_R = 10 \text{ mm}, \quad r_{I1} = 3 \text{ mm}, \quad r_{I2} = 5 \text{ mm}. \tag{75}$$

At the inlet area, initial temperature and pressure, the inner and outer volume fluxes, the corresponding velocity profile and mass fractions are

$$T = 1{,}200°\text{C}, \qquad p = 1 \text{ bar}. \tag{76}$$

$$\dot V_I = 304 \text{ cm}^3/\text{min} \qquad \dot V_O = 7{,}002.4 \text{ cm}^3/\text{min} \tag{77}$$

$$Y_1^I = 2.02\times10^{-3} \qquad Y_1^O = 0 \tag{78}$$

$$Y_2^I = 0 \qquad Y_2^O = 2.65\times10^{-3} \tag{79}$$

$$Y_3^I = 0 \qquad Y_3^O = 0 \tag{80}$$

$$Y_4^I = 0.99798 \qquad Y_4^O = 0.99735 \tag{81}$$

$$v_z = \begin{cases} \dfrac{2\dot V_I}{\pi r_{I1}^4}\left(r_{I1}^2 - r^2\right) & \text{for } 0 \le r \le r_{I1} \\ 0 & \text{for } r_{I1} < r < r_{I2} \\ \dfrac{2\dot V_O}{\pi\left(r_R^2 - r_{I2}^2\right)} \dfrac{\left(r^2 - r_{I2}^2\right)\ln\left(r_R/r_{I2}\right) - \left(r_R^2 - r_{I2}^2\right)\ln\left(r/r_{I2}\right)}{r_R^2 - r_{I2}^2 - \left(r_R^2 + r_{I2}^2\right)\ln\left(r_R/r_{I2}\right)} & \text{for } r_{I2} \le r \le r_R. \end{cases} \tag{82}$$

The transport properties of the gaseous species were calculated based on hard-sphere radii, which were determined from their measured viscosities:

$$r_{NH_3} = 1.994\times10^{-10} \text{ m}, \quad r_{SiCl_4} = 4.328\times10^{-10} \text{ m},$$
$$r_{HCl} = 2.128\times10^{-10} \text{ m}, \quad r_{N_2} = 2.030\times10^{-10} \text{ m}.$$

In the case of $SiCl_4$, no viscosity data were found and the experimental data for the binary diffusion of $SiCl_4$ in air were used.

In Figures 2 and 3 the radial profiles of the velocity, the temperature, and the mass fractions near the inlet ($z \approx 1$ cm) are shown. The two parabolic inlet velocity profiles can still be identified. The temperature profile has a minimum at the

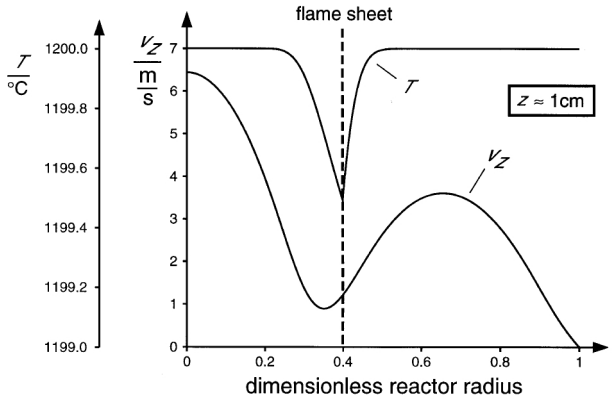

Figure 2. Temperature and velocity near the inlet.

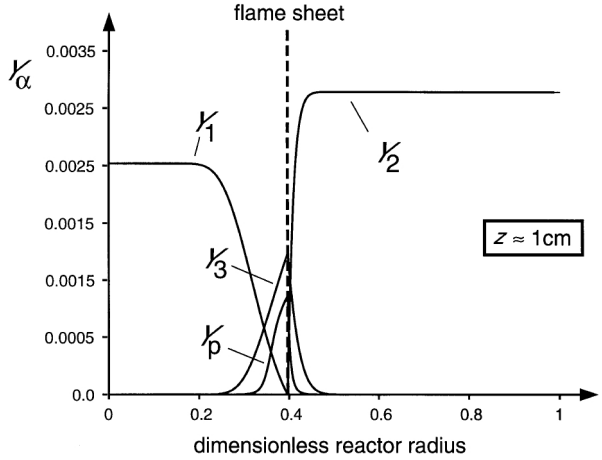

Figure 3. Mass fractions near the inlet.

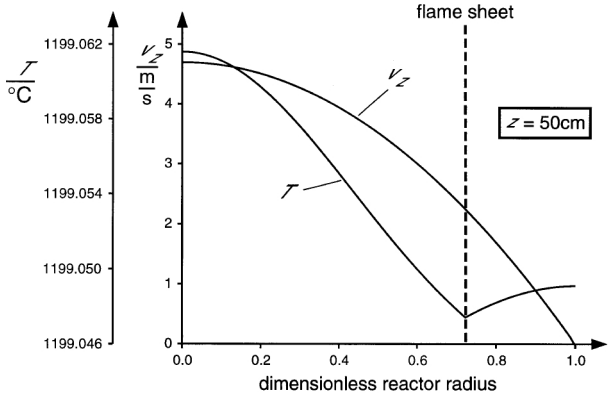

Figure 5. Temperature and velocity at the outlet.

radial position of the flame sheet because the reaction is endothermic. Since the reaction enthalpy and the mass fractions of the precursors are low, the decrease in temperature due to chemical reaction amounts only to about half a Kelvin. The mass fractions of the products HCl (Y_3) and the particle phase (Y_p) have a maximum there. The profiles of the precursors NH_3 (Y_1) and $SiCl_4$ (Y_2) are zero at the flame sheet.

Figure 4 shows for $z \approx 1$ cm the radial profiles of the mean particle radius r_g and its standard deviation σ. At the flame sheet, the reaction process yields small particles and coagulation produces larger particles. The combination of these effects leads to a broad spectrum of $N(r_p)$ resulting in a maximum of σ. Near the flame sheet, the particle density as well as coagulation activity are high causing comparatively large values for r_g. Only at the flame sheet itself there is a slight local minimum that is caused by the supply of small particles due to the chemical reaction. Left and right of this local minimum are local maxima, where the left one is significantly higher. Due to the cylindrical geometry the particle density is higher at smaller radii. This results in a higher coagulation rate yielding larger particles. Accordingly, the gradient of the mass fraction of the particles is at the left side of the maximum and is not so steep as at the right side.

Figures 5, 6 and 7 show the profiles of the characteristic quantities at the outlet of the reactor ($z = 50$ cm). The velocity has a parabolic Hagen–Poiseuille-like profile and the temperature is nearly constant. The radial position of the minimum of the temperature profile is again the flame-sheet position. The mass fraction Y_3 (HCl) is nearly constant and almost homogeneously distributed. The mass fraction Y_p of the particle phase is completely different. Only in the radius range in the middle, over which the flame sheet has moved at lower z-values, Y_p reaches comparatively high values. At both edges of this radius range, the Y_p-curve slopes down rapidly, and outside of this range Y_p is nearly zero. This peculiarity needs some further explanation: the reduction of the reaction zone to a sheet with a comparatively high reaction rate produces a high particle density resulting in a high coagulation activity in this region. The particles grow rapidly up to a size, where their capability for diffusion has decreased considerably because the diffusion coefficient in the free molecular regime is proportional to $1/r_p^2$. Practically, these particles are transported only by convection. In the confined pipe flow, the velocity is nearly parallel to the reactor axis. Hence, convection only induces particle transport in the axial direction, and transport in the radial direction plays only a secondary role. The radial profiles of r_g and σ (Figure 7) show qualita-

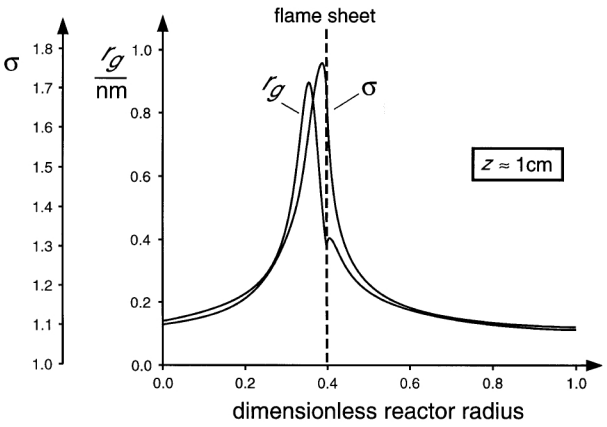

Figure 4. Geometric mean radius and standard deviation near the inlet.

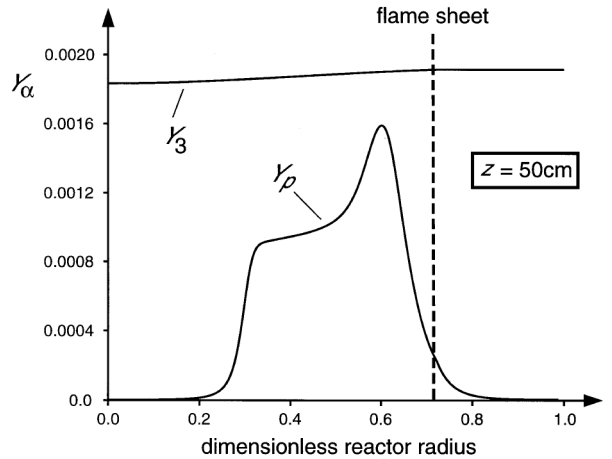

Figure 6. Mass fractions at the outlet.

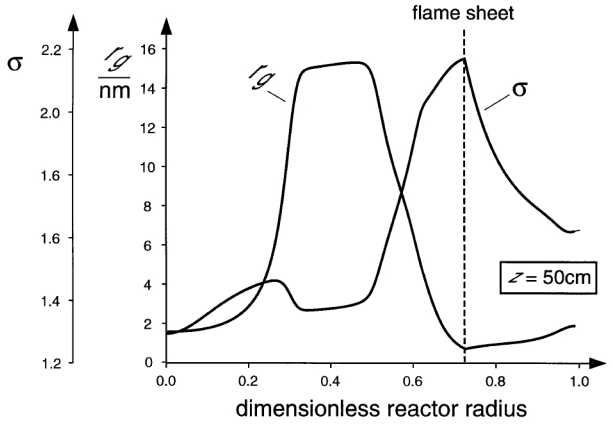

Figure 7. Geometric mean radius and standard deviation at the outlet.

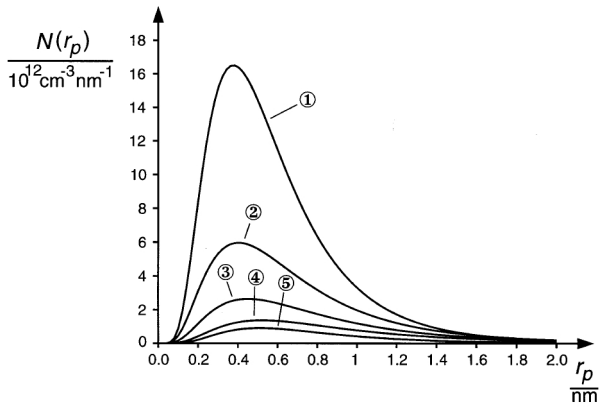

Figure 9. Development of the size distribution along the flame sheet.

tively the same features as near the inlet (Figure 4). In the range of the dimensionless reactor radius of around 0.4 where particles have been produced first, that is, near the inlet, the coagulation process lasted the longest period and hence there are the largest particles with a mean radius of about 15 nm. In this range σ reaches values of about 1.35, which is close to a self-preserving size distribution (Lai et al., 1972).

Figure 8 shows the calculated position of the flame sheet in the tubular reactor. The frame of the plot represents the inlet, outlet, and wall of the reactor. Also marked are several points inside the reactor at which the size distributions have been calculated; these are shown in Figures 9 to 11. The development of the size distribution along the flame sheet is represented in Figure 9. The number density is obviously dominated by the particles that are newly formed in the flame sheet resulting in particles of small mean radii. The reaction rate decreases along the sheet and so does the total number density of the particles. A different development of the size distribution can be observed along the middle axis of the reactor, as shown in Figure 10. Coagulation results in a decrease of the total particle number density of the particles along the axis, on the one hand, and in an increase of the mean radius, on the other hand. Figure 11 shows size distributions at different radial positions at the outlet area of the reactor. Point 11 is closest to the flame sheet. The corresponding distribution is mainly influenced by newly formed particles. Its mean radius r_g still has a comparatively low value of about 6.4 nm. Point 12 has the radial position of the flame sheet at the inlet (see Figure 8). Here those particles are found that were produced near the inlet and that had the most time to grow by coagulation. So, r_g here reaches its maximum value of about 15 nm, and the largest particles are found here. Point 13 is outside the radius range that the flame sheet has passed, that is, at this radial position particles never have been produced. So particles can reach this position only by diffusion. Since diffusion favors small particles, we find here smaller particles again, with values of $r_g \approx 5$ nm. This holds so much more for point 14 at the wall. The high coagulation activity of the particles arriving at point 12 results in a lower total number density than in points 13 and 14.

Discussion

The results reveal the clear influence of chemical reaction and coagulation on the spatial distribution and composition of particles inside the reactor. The location of the reaction zone in combination with convective transport and radial dif-

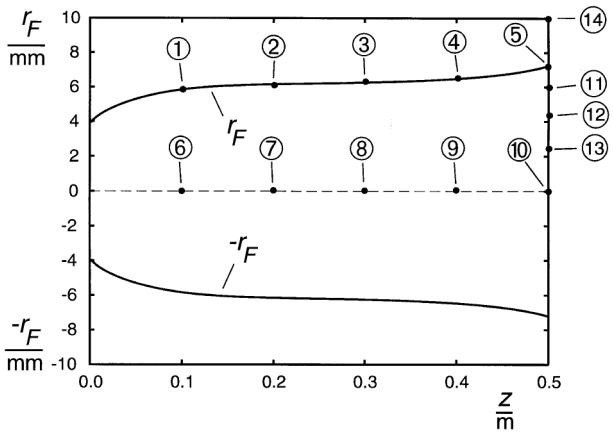

Figure 8. Location of the flame sheet in the reactor.

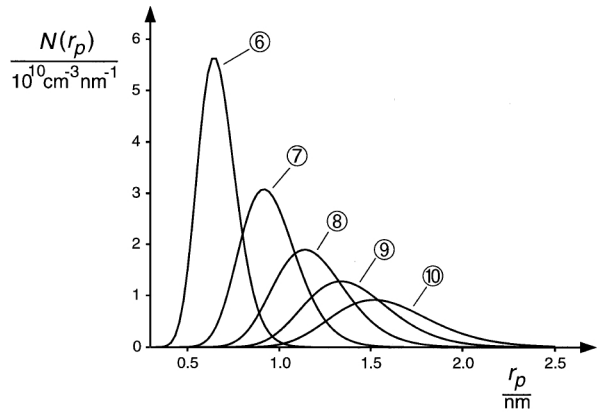

Figure 10. Development of the size distribution along the middle axis.

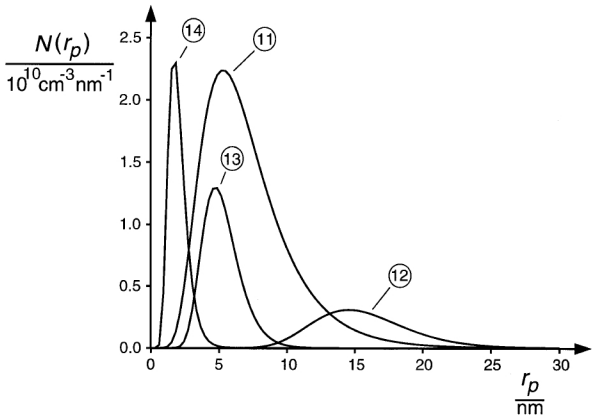

Figure 11. Size distribution at different radial positions at the outlet.

fusion mainly determine where particles can be found. In the preceding flow regime, which is basically parallel to the symmetry axis, particles leave the reactor predominantly at those radial positions that have been passed by the reaction zone inside the reactor. There the mass fraction of the particle phase is significantly higher (Figure 6) and their average size is larger (Figure 7) than outside of this radial region. The model presented here incorporates all relevant effects to describe these phenomena in detail. It allows calculation of the formation and growth of particles in a gas-phase reactor where the reaction processes are diffusion controlled, and it includes convective and diffusive particle transport. Due to the spacial inhomogeneity of the reactor, the standard deviation σ varies significantly even within the outlet cross section, as can be seen from Figure 7. In particular, in reactor volumes near the flame sheet, the standard deviation reaches values of $\sigma > 2$. In this case, the usual approximation of the collision integral becomes questionable. This is the reason for using the improved approximation, given in the Appendix.

It should be noticed that even at the outlet after a distance of 500 mm the mean particle radius does not exceed a value of 15 nm. Three reasons may account for this low value. First, the mass fraction of the precursors at the inlet is quite low, being on the order of 10^{-3}. Second, the process is laminar and diffusion controlled, which slows down the particle formation and the subsequent growth. Third, the flame sheet walks through the whole reactor, producing particles of very small size even at the outlet.

Acknowledgment

The authors express their sincere appreciation to the Bundesministerium für Bildung, Wissenschaft, Forschung und Technologie of the German government for the financial support.

Literature Cited

Chase, M., C. Davies, J. Downey, D. Frurip, R. McDonald, and A. Syverud, "JANAF Thermochemical Tables," *J. Phys. Chem. Ref.*, **14** (1985).

Chung, S., and J. Katz, "The Counter Flow Diffusion Flame Burner: A New Tool for the Study of the Nucleation of Refractory Compounds," *Comb. Flame*, **61**, 100 (1985).

Danforth, S., "Synthesis and Processing of Untrafine Powders for Si_3N_4 Ceramics," *Nanostr. Mat.*, **1**, 197 (1992).

Friedlander, S., *Smoke, Dust and Haze*, Wiley, New York (1977).

Hirschfelder, J., C. Curtiss, and R. Bird, *Molecular Theory of Gases and Liquids*, Wiley, New York (1954).

Janiga, J., K. Sin, and V. Figusch, "Synthesis of Silicon Nitride Powders by Gas-Phase Reaction," *J. Eur. Ceram. Soc.*, **8**, 153 (1991).

Kim, K., "Analysis of SiO_2 Particle Generation and Deposition Using Tube Furnace Reactors," *AIChE J.*, 2679 (1997).

Kizaki, Y., T. Kandori, and Y. Fujitani, "Synthesis and Characterization of Si_3N_4 Powder Produced by Laser-Induced Chemical Reaction," *Jap. J. Appl. Phys.*, **24**, 800 (1985).

Kruis, R., W. Oostra, J. Marijnissen, J. Schoonman, and B. Scarlett, "Particle Formation Paths in the Synthesis of Silicon Nitride Powder in a Laser-Heated Aerosol Reactor," *J. Eur. Ceram. Soc.*, **18**, 1025 (1998).

Lai, F., S. Friedlander, and J. Pich, "The Self-Preserving Size Distribution for Brownian Coagulation in the Free-Molecular Regime," *J. Colloid Interface Sci.*, **39**, 395 (1972).

Lee, K., H. Chen, and J. Gieseke, "Log-Normally Preserving Size Distribution for Brownian Coagulation in the Free-Molecular Regime," *Aerosol Sci. Technol.*, **3**, 53 (1984).

Lee, K., Y. Lee, and D. Han, "The Log-Normal Size Distribution Theory for Brownian Coagulation in the Low Knudsen Number Regime," *J. Colloid Interface Sci.*, **188**, 486 (1997).

Mathur, S., P. Tondon, and S. Saxena, "Thermal Conductivity of Binary, Ternary and Quaternary Mixtures of Rare Gases," *Mol. Phys.*, **12**, 569 (1967).

Otto, E., H. Fissan, S. Park, and K. Lee, "Brownian Coagulation in the Transition Regime Using the Moments of a Log-Normal Distribution," *J. Aerosol Sci.*, **28**, 629 (1997).

Pratsinis, S., "Simultaneous Nucleation, Condensation, and Coagulation in Aerosol Reactors," *J. Colloid Interface Sci.*, **124**, 416 (1988).

Pratsinis, S., and S. Mastrangelo, "Material Synthesis in Aerosol Reactors," *Chem. Eng. Prog.*, **85**, 62 (1989).

Prochazka, S., and C. Greskovich, "Synthesis and Characterisation of a Pure Silicon Nitride Powder," *Ceram. Bull.*, **57**, 579 (1978).

Ulrich, G., "Theory of Particle Formation and Growth in Oxide Synthesis Flames," *Combust. Sci. Technol.*, **4**, 47 (1971).

Ulrich, G., "Flame Synthesis of Fine Particles," *Chem. Eng. News*, **62**, 1 (1984).

Whitby, E., P. McMurry, U. Shankar, and F. Binkowski, "Modal Aerosol Dynamics Modelling," *EPA Rep.*, pp. 600/3–91/020 (1991).

Xing, F., Ü. Ö. Köylü, and D. Rosner, "Synthesis and Restructuring of Inorganic Nanoparticles in Counterflow Diffusion Flames," *Comb. Flame*, **107**, 85 (1996).

Appendix

The collision integral in Eq. 17 cannot be calculated analytically. However, an analytical expression is needed. So the integrand has to be skillfully approximated, which has been attempted by several authors (see Pratsinis, 1988; Otto et al., 1997). An alternative approximation is described below and compared with previous results.

The exact integrand reads

$$f(y) = \left[1 + \exp\left(2\sqrt{Z}\,y\right)\right] \cosh^{1/2}\left(3\sqrt{Z}\,y\right) \exp\left(-y^2\right) \quad \text{(A1)}$$

$$Z = \ln^2 \sigma\,. \quad \text{(A2)}$$

The analytical integration cannot be performed because of the square-root term. For this term Pratsinis (1988) chooses the approximation,

$$\cosh^{1/2}\left(3\sqrt{Z}\,y\right) \approx \sqrt{2}\left(0.633 + 0.092\,\sigma^2 - 0.022\,\sigma^3\right) \times \cosh\left(\frac{3}{2}\sqrt{Z}\,y\right), \quad \text{(A3)}$$

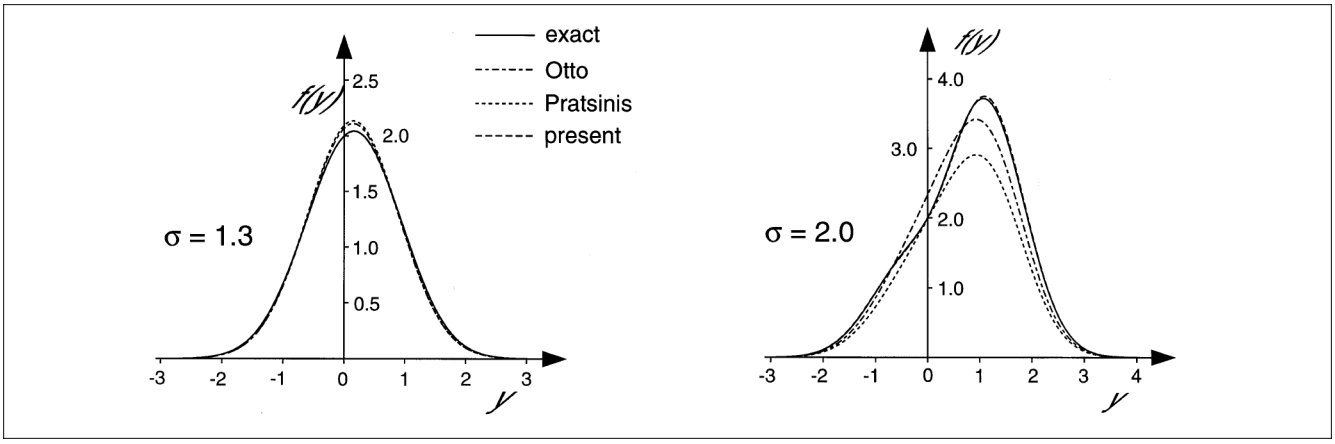

Figure A1. Exact and approximated integrands.

Otto et al. (1997) uses the approximation,

$$\cosh^{1/2}\left(3\sqrt{Z}\,y\right) \approx \sqrt{2}\left[1+1.2\exp\left(-2\sigma\right) - 0.646\exp\left(-0.35\sigma^2\right)\right]\cosh\left(\frac{3}{2}\sqrt{Z}\,y\right), \quad \text{(A4)}$$

while the authors found the approximation:

$$\cosh^{1/2}\left(3\sqrt{Z}\,y\right) \approx \left[\sqrt{2}+\left(1-\sqrt{2}\right)\exp\left(-\left(\frac{3}{2}\sqrt{Z}\,y\right)^2\right)\right] \times\cosh\left(\frac{3}{2}\sqrt{Z}\,y\right). \quad \text{(A5)}$$

Figure A1 shows the exact integrand and the three approximations for two typical values of σ. While the present approximation is practically identical with the exact integrand, the other two approximations show distinct deviations. For larger but still realistic values of σ, the approximation of Pratsinis (1988) deviates more and more from the exact form until it even changes the sign. On the other hand, the deviation of the approximation of Otto et al. (1997) decreases for increasing values of σ. Only if the present approximation is used one can be sure that deviation of the results presented here are due to the assumption of the model itself and not to the approximations in evaluating the model.

Manuscript received Nov. 23, 1998, and revision received June 28, 1999.